Electron-impact ionization of Sm^{12+} ions: Resonances far beyond threshold

D. M. Mitnik and D. C. Griffin
Department of Physics, Rollins College, Winter Park, Florida 32789

J. Colgan and M. S. Pindzola
Department of Physics, Auburn University, Auburn, Alabama 36849

K. Aichele, W. Arnold, D. Hathiramani, F. Scheuermann, and E. Salzborn
Institut für Kernphysik, University of Giessen, D–35392 Giessen, Germany
(Received 5 June 2001; published 14 November 2001)

Unusual resonance features at high energies were recently discovered in the experimental crossed-beams measurements of the electron-impact ionization of Sm^{12+}. Theoretical calculations were able to confirm that they are due to deep-core excitation with capture into dielectronic states followed by sequential double Auger decay [K. Aichele *et al.*, Phys. Rev. Lett. **86**, 620 (2001)]. In this paper additional experimental results are presented, showing more resonances in the single-ionization cross section. Detailed level-to-level calculations of dielectronic capture provide a clear identification of these resonances, as produced by a $3d$-$4f$ excitation with capture to different nl orbitals followed by sequential emission of two electrons. By using configuration-average distorted-wave calculations, we estimate the branching ratios for single and double ionization by considering the possible autoionization paths leading to resonant contributions to excitation, single ionization, and double ionization.

I. INTRODUCTION

Electron-impact ionization is one of the most important atomic processes in astronomical and laboratory plasmas. Both the direct ionization process and the indirect process of excitation-autoionization (EA) have been studied extensively. A summary of the theoretical work and comparisons with experiment for the indirect EA process can be found in Ref. [1]. An additional indirect ionization process was first postulated by LaGattuta and Hahn [2]. It involves dielectronic capture of the incident free electron with simultaneous excitation of an inner-shell electron followed by sequential emission of two electrons. This three-step mechanism was termed resonant-excitation double autoionization (REDA) and is characterized as a series of resonances converging to the steplike threshold of an EA feature.

This higher-order process has been studied in detail in ions having relatively few (about 10) electrons. For example, in Refs. [4–6], large REDA contributions to the total ionization cross sections are presented and detailed comparisons between experimental measurements and theoretical calculations for the resonance structures are provided. Moreover, in these cases, the REDA contributions to electron-impact ionization occur in an energy region close to the ionization threshold. Both the EA and REDA contributions have a monotonic decreasing behavior with respect to the incident electron energy, and at high energies where the direct mechanism should dominate, the ionization cross section is expected to be smooth.

Recently, however, unusual features have been discovered [3] at high incident electron energies for the single-ionization cross sections of atomic ions with charge states of up to 13+ in the Pr and Sm rare-earth isonuclear sequences. These resonances are found at energies of about four times the threshold energy for single ionization. Preliminary theoretical calculations [3] identified these resonances as produced by a deep-core inner-subshell excitation with electron capture, followed by sequential double autoionization. In the present work, we focus on the Sm^{12+} ion and use level-to-level distorted-wave calculations to identify and map the recombination resonances features. We then employ the configuration-average distorted-wave approximation to estimate the branching ratios for the contributions of the dielectronic capture processes to the single and double ionization of Sm^{12+}. The remainder of this paper is arranged as follows: In Sec. II, we describe the crossed-beams experiment and show the experimental results for the electron-impact ionization of Sm^{12+}. In Sec. III, we review the different processes that contribute to the electron-impact ionization of atomic ions. In Sec. IV, we present the results of the theoretical calculations and identify the high-energy features. Finally, in Sec. V, we provide a brief summary.

II. EXPERIMENTAL RESULTS

Experimental measurements and theoretical calculations of the electron-impact ionization cross section of Sm^{12+} have been presented in Ref. [3]. The measurements were performed using the crossed electron-ion beams setup at the University of Giessen. More complete discussions of the experimental methods employed are presented in Ref. [7] and for the Sm isonuclear sequence in Ref. [8].

The Sm ions were produced in the plasma of a 10 GHz electron-cyclotron-resonance (ECR) ion source using an evaporation oven. The ions were extracted with energies of $q \times 10$ keV, separated magnetically for the desired mass-to-charge ratio, and collimated before they were crossed with an intense electron beam at an angle of 90°. The electron gun
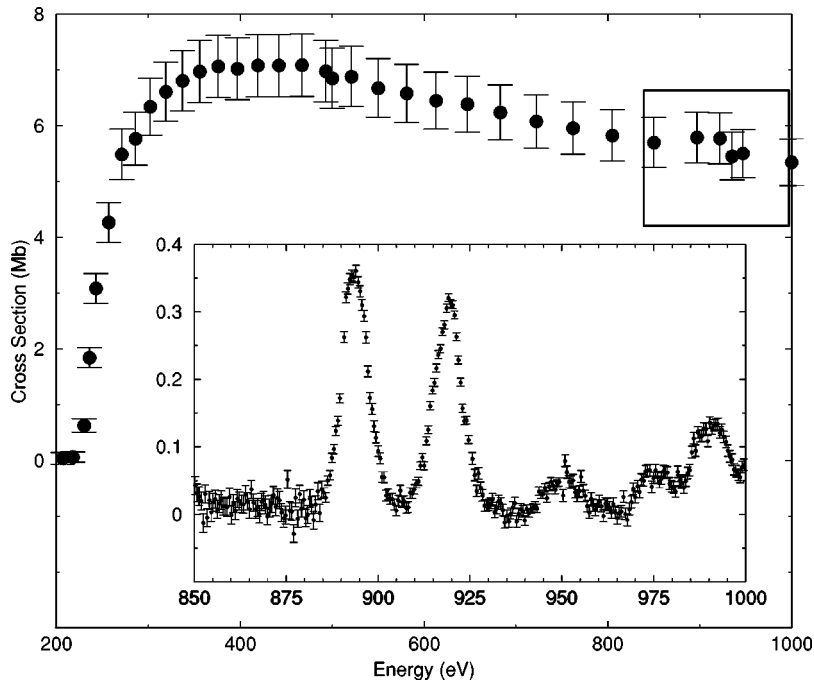
FIG. 1. Total cross section for the electron impact single ionization of Sm^{12+}. The inset shows the REDA resonances from 850 eV to 1000 eV, after subtracting the smooth background cross section.

supplies electrons with energies between 10 eV and 1 keV with currents up to 430 mA [9].

The dynamic crossed-beams technique was used to obtain absolute cross sections [10], where the electron beam passes through the ion beam while the count rate of ionized ions, the electron and the ion current, and the speed of the movement are recorded simultaneously in four different multichannel analyzer spectra with typically 512 channels each. Due to fluctuations of the experimental parameters during the measurement, one cross-section value cannot be reproduced to better than 0.5% by a longer measurement time. Therefore, this method is not suitable for resolving small features in the cross section.

For high-resolution measurements another mode, the energy-scan method, was employed [11]. In this mode, we leave the electron gun in a fixed position with an optimum electron-ion beam overlap. The same parameters are measured as for the dynamic crossed-beams method, with simultaneous variation of the electron energy in steps of typically 0.08 eV and measurement times for each channel of 20 ms. Changing the energy and providing the necessary gate signal from the computer takes about 0.2 ms. One scan spans typically over 40 eV. By repeating the scans thousands of times, we average out possible fluctuations in the beam overlap, (i.e., the form factor), the measurement of beam currents, and count rates. This is done until the counting statistic reaches a desired level. Numerous individual overlapping energy scans are then combined, and the final relative scan measurement is obtained. The electron energy is limited by the maximum cathode voltage that can be applied to the electron gun and is below 1000 eV. A separate measurement with the same beam parameters and adjustments without beam overlap gives the background of the ionization signal needed for the analysis.

During the measurement, the space charge of the electron beam is compensated with slow ions from Kr gas fed into the collision region; therefore, no energy correction for the

analysis is needed. Furthermore, this gives us a better energy resolution than a measurement without space charge compensation. The error of the experimental energy scale is within 1.5 eV [12]. The energy resolution is measured for isolated resonances at Li-like Ne^{7+} ions and is found to be around 3 eV at an electron energy of 950 eV [13].

In Fig. 1, we show the absolute cross section for single ionization of Sm^{12+}, measured with the dynamic crossed-beams method. A small deviation of two data points at around 897 and 922 eV can be seen in the smooth high-energy cross section. This prompted us to perform an additional energy-scan measurement between 850 and 1000 eV, and the results are shown in the inset of the figure. Unusual resonances are found well above the threshold energies associated with the major direct and indirect contributions to single ionization of Sm^{12+}. We have subtracted the background contribution to single ionization to isolate the resonances. This procedure involves a small uncertainty of the overall size of the result, since the nonresonant contributions cannot be measured separately. It is important to note that this cannot be done without large uncertainties at lower energies or in the threshold region, where there are many excitation-autoionization thresholds. The energy-scan results show a rich spectrum of peaks starting at 893 eV. The first peak, which is the strongest observed, contributes $\approx 6.5\%$ to the total cross section.

If these peaks are from autoionizing states formed after inner-shell excitation with capture of the incident electron, it should be possible to observe corresponding resonances in the double-ionization cross section. This implies the emission of three electrons. Therefore, we performed similar measurements for the double-ionization of Sm^{12+} between 880 and 935 eV, which have been already presented in Fig. 4 of Ref. [3]. The relative resonant contribution to the the double ionization cross section increases to 11.8% for the

first peak. In similar measurements for Sm^{11+}, which are not shown, we also found that the resonance features occur at the same energy in the single and double-ionization cross sections.

There are several potential errors in measurement that could be thought to cause uncertainties in the observation of resonance effects. First, a change of the contact potentials of the connectors at the electron gun will give systematic errors. However, this was not observed at any time. Another potential error could be the changing of the cathode position of the electron gun due to a thermic expansion relative to the pierce electrode. We know from position tests that this affects the emission and the trajectory of the electrons. This can also be neglected because we have measured similar double-ionization resonance peaks for Sm^{11+}, using the same electron gun, and they show no energy shift compared to the single ionization resonances of Sm^{11+}. Finally, the effect of an uncompensated space charge of the electron beam can be neglected. Therefore, our measurements show strong experimental evidence that the observed structure results from a resonant process. We now turn our attention to the theoretical methods employed in our calculations.

III. CALCULATIONAL PROCEDURE

Major contributions to the electron-impact single-ionization cross section are made by the following two processes:

$$e^- + A^{q+} \rightarrow A^{(q+1)+} + e^- + e^-, \tag{1}$$

and

$$e^- + A^{q+} \rightarrow (A^{q+})^* + e^- \rightarrow A^{(q+1)+} + e^- + e^-, \tag{2}$$
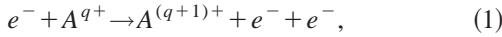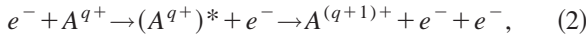
where A^{q+} represents an arbitrary ion with charge q, and the asterisk represents an inner-shell excited level. The first process is direct ionization (DI) while the second is excitation-autoionization (EA). The equations for treating these processes using the independent processes approximation are given, for example, in Ref. [8].

An additional process that can contribute to the single-ionization cross section is the following:

$$e^- + A^{q+} \rightarrow (A^{(q-1)+})^{**} \rightarrow (A^{q+})^* + e^- \rightarrow A^{(q+1)+} + e^-$$
$$+ e^-, \tag{3}$$
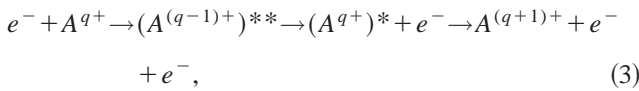
where $(A^{(q-1)+})^{**}$ represents an intermediate autoionizing level populated by inner-shell excitation with capture of the incident electron. If this is followed by two successive autoionizations as shown above, it contributes to the single-ionization cross section. This process is called resonant excitation double autoionization (REDA) [2], and the corresponding cross section is given by

$$\sigma_{REDA}(g \rightarrow f) = \sum_d \sigma_C(g \rightarrow d) \sum_j B_a(d \rightarrow j) B_a(j \rightarrow f). \tag{4}$$

In Eq. (4) $B_a(d \rightarrow j)$ is the branching ratio for autoionization from level d to level j, and is defined by

$$B_a(d \rightarrow j) = \frac{A_a(d \rightarrow j)}{\sum_k A_a(d \rightarrow k) + \sum_m A_r(d \rightarrow m)}, \tag{5}$$

where $A_a(d \rightarrow k)$ is the autoionizing rate in Hz from level d to level k, and $A_r(d \rightarrow m)$ is the radiative rate in Hz from level d to any lower-energy level m. For the ions studied in this work we found that in general the radiative rates are much smaller than the autoionization rates, therefore, we apply the approximation of neglecting the radiative rates A_r in the calculation of the branching ratios [Eq. (5)]. $\sigma_C(g \rightarrow d)$ is the energy-averaged dielectronic-capture cross section from level g to level d of the (N+1)-electron ion and is given by

$$\sigma_C(g \rightarrow d) = \frac{(2\pi a_0)^2 (I_H)^2}{\Delta E E_{dg}} \frac{g_d}{2g_g} A_a(d \rightarrow g), \tag{6}$$

where E_{dg} is the relative energy (between the captured level d and the initial level g, respectively), g_d and g_g are the statistical weights of levels d and g, respectively, $(2\pi a_0)^2 = 2.6741 \times 10^{-32}$ cm^{2}s, and I_H is the ionization potential of the hydrogen atom. The energy bin width ΔE is chosen to be larger than the largest resonance width, but much smaller than the experimental width. Finally, smooth theoretical cross sections curves are generated by convoluting the spectrum of narrow resonance peaks with a Gaussian for which the full width at half maximum (FWHM) is equal to the experimental width.

To identify the high-lying resonances in the experimental data, a detailed level-to-level calculation of the capture cross section σ_C is required. We calculated the atomic structure of the deep-inner-shell excited levels and the autoionization rates using the HULLAC package [14]. In this package, the level energies are calculated using the fully relativistic multiconfigurational RELAC code [15], based on the parametric potential model [16]. The central potential is introduced as an analytic function of screening parameters that are determined by minimizing the first-order relativistic energy of a set of configurations. The level-to-level autoionization rates needed to determine $\sigma_C(g \rightarrow d)$ are calculated using the relativistic distorted-wave approximation.

As we will show in the next section, for deep-inner-shell excitations, the electron capture can populate configurations of the recombined ion that are well above the first ionization limit of the initial ion. This may be followed by radiative transitions to bound states of the recombined ion, thereby completing the dielectronic recombination process. However, recombination into these highly excited states may also be followed by a series of autoionizing transitions. These autoionization processes can populate bound states of the initial ion through the emission of a single electron, resulting in a resonant contribution to excitation; or they can contribute to single ionization through the emission of two electrons, or multiple ionization through the emission of three or more electrons. Due to the very complex nature of the atomic structure of Sm^{12+}, the configuration-average distorted-wave
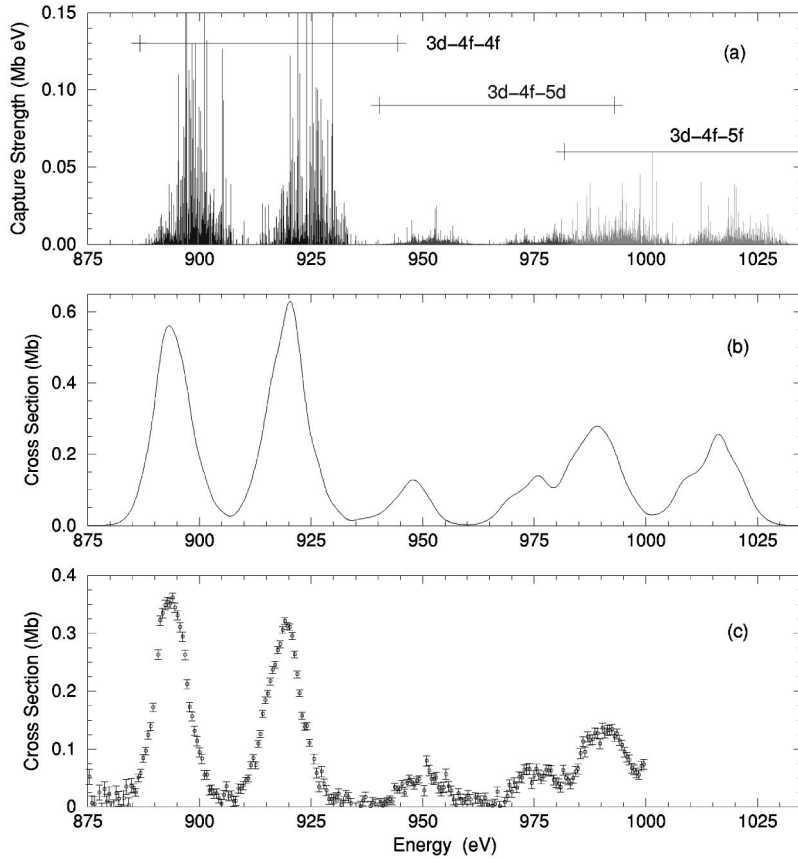
FIG. 2. (a): Dielectronic capture strengths to the $3d^9 4s^2 4p^6 4d^{10} 4f^4 5s^2$ $(3d-4f-4f)$, $3d^9 4s^2 4p^6 4d^{10} 4f^3 5s^2 5d$ $(3d-4f-5d)$, and $3d^9 4s^2 4p^6 4d^{10} 4f^3 5s^2 5f$ $(3d-4f-5f)$ excited configurations. (b): Total dielectronic capture convoluted with a 3 eV width (FWHM) Gaussian. The calculation includes the $3d-4f-4f$, $3d-4f-5p$, $3d-4f-5d$, $3d-4f-5f$, $3d-4f-6p$, and $3d-5p-5p$ processes. (c): Experimental measurements for single ionization REDA resonances of Sm^{12+} (background reduced).

approximation (CADW) is the only method that is feasible in a calculation of these possible autoionizing paths. In the CADW approximation [17], the first-order scattering amplitude is averaged over all states of the initial configuration and summed over all states of the final configuration. The bound-state energies and the atomic orbitals for the many configurations needed to evaluate the rates are generated using the radial wave-function code developed by Cowan [18]. These radial wave functions are solutions to the Hartree-Fock equations and the continuum orbitals needed to evaluate the Coulomb matrix elements are calculated in a local distorting potential constructed in a semiclassical exchange approximation [19].

IV. RESULTS

A. Calculation of dielectronic capture cross sections and identification of the resonant contributions

Our previous calculations of electron-impact ionization of Sm^{12+} [8] show that the ion beam is an unknown mixture of the ground level and the many long-lived metastable levels found in the ground and low-lying excited configurations. Comparisons of the CADW results for the dielectronic capture from the $[Kr] 4d^{10} 4f^2 5s^2$ ground configuration with dielectronic capture from the $[Kr] 4d^{10} 4f^3 5s$ and $[Kr] 4d^{10} 4f^4$ excited configurations (containing metastable levels) have been presented in Ref. [3]. Although the experimental beam is an unknown mixture of ground and metastable configurations, we discuss here theoretical results from the ground

configuration only; this is justified by the fact that our previous CADW calculations for capture from excited configurations containing metastable levels were similar to those for capture from the ground configuration [3].

Detailed level-to-level calculations performed with the HULLAC code suggest that the strong resonance features shown in Fig. 1 are produced by capture to the $3d^9 4s^2 4p^6 4d^{10} 4f^4 5s^2$ configuration of Sm^{11+}. This configuration has 977 levels spread between 890 eV and 945 eV (relative to the ground state). The electron capture from the ground state of Sm^{12+} to this level is a resonant process in which a free electron induces the excitation even though it has an energy significantly lower than the $3d$-$4f$ excitation threshold of approximately 1100 eV. Since the incoming electron does not have enough energy to escape, it is captured, in this case, into the $4f$ orbital. We label this process as $3d-4f-4f$, denoting the $3d-4f$ excitation with capture into the $4f$ orbital.

In order to calculate the dielectronic capture strength $(\sigma_C \Delta E)$ into the $3d^9 4s^2 4p^6 4d^{10} 4f^4 5s^2$ configuration, we performed detailed level-to-level calculations, which are presented in Fig. 2(a). We find a bimodal distribution in the capture strength separated by about 27 eV which corresponds to the spin orbit splitting between the $3d_{3/2}$ and $3d_{5/2}$ levels of the $3d^9 4s^2 4p^6 4d^{10} 4f^4 5s^2$ configuration. To confirm this, we calculated the energy levels of the $3d^9 4s^2 4p^6 4d^{10} 5s^2$ configuration of Sm^{15+}, and obtained a value of 25.8 eV for the fine-structure splitting of the $3d_J$ levels. To compare with our CADW results, we also averaged the detailed level-to-
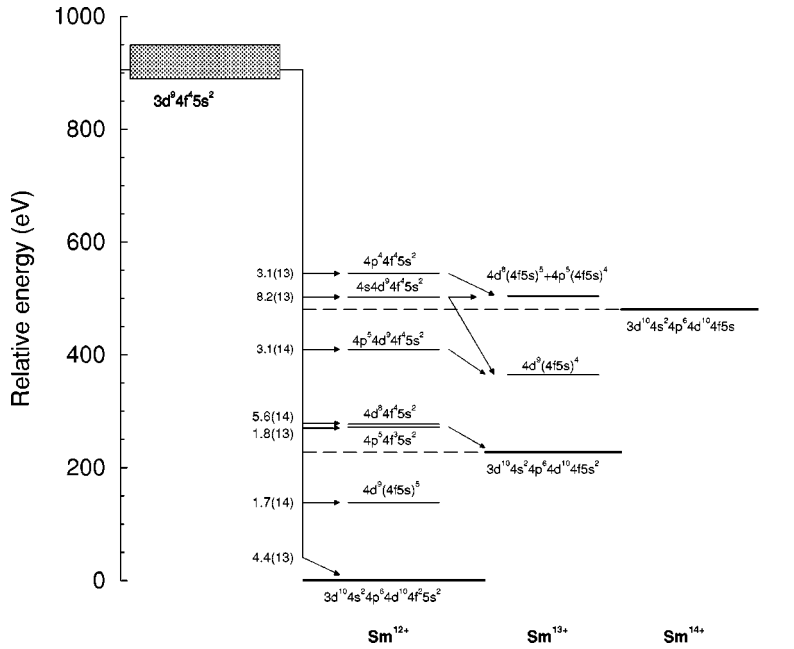
FIG. 3. Energy-level diagram and main auto-ionization channels involved in the resonant-excitation multiple-autoionization processes through the $3d^94s^24p^64d^{10}4f^45s^2$ configuration (labelled as $3d^94f^45s^2$). In order to simplify the notation, all the closed subshells are suppressed in the labeling of the excited configurations. In addition, the notation such as $4d^9(4f5s)^5$ refers to the configurations $3d^{10}4s^24p^64d^94f^35s^2$, $3d^{10}4s^24p^64d^94f^45s$ and $3d^{10}4s^24p^64d^94f^5$.

level results, and obtained an average energy of 908 eV with an average autoionization rate of 4.1×10^{13} Hz. Using these values and Eq. (6), with $g_d=10\,010$ and $g_g=91$, we obtained an average dielectronic capture strength of 12.3 Mb eV. The averaged-configuration dielectronic capture strength, calculated from the CADW codes is 13.2 Mb eV. Alternatively, the average capture strength can be extracted from the detailed results by calculating the capture to all the individual levels in the configuration, summing over all the resonances, and then averaging over the levels of the initial configuration. Using this approach the resulting configuration-averaged capture strength is 12.1 Mb eV.

We have also examined other possible processes that can produce REDA resonances in this energy region. We found a noticeable contribution in the dielectronic capture cross section from the $3d-4f-5d$ and $3d-4f-5f$ processes, which are also displayed in Fig. 2(a). In this part of the figure, only transitions from the ground state $3d^94s^24p^64d^{10}4f^25s^2$ [$J=4$] are shown. The $3d^94s^24p^64d^{10}4f^35d$ configuration (the final configuration in the $3d-4f-5d$ process) consists of 3565 levels spread between 940 eV and 993 eV. The $3d^94s^24p^64d^{10}4f^35f$ configuration (the final configuration in the $3d-4f-5f$ process) consists of 4703 levels spread between 982 eV and 1040 eV. It is clear that these configurations also show a bimodal distribution, again produced by the spin-orbit splitting of the $3d$ orbitals.

Detailed calculations of the total dielectronic capture cross-section through the $3d-4f-4f$, $3d-4f-5d$, $3d-4f-5f$, and the additional $3d-4f-5p$, $3d-4f-6s$, and $3d-5p-5p$ processes, convoluted with a 3 eV width (FWHM) Gaussian, are shown in Fig. 2(b), along with experimental measurements for REDA, shown in Fig. 2(c) . We calculated the capture strength from an average of the 13 levels of the $3d^{10}4s^24p^64d^{10}4f^25s^2$ ground configuration of Sm^{12+} to each of the 13 752 levels of the final configurations. The resultant capture strengths were then convoluted

with a 3 eV width (FWHM) Gaussian distribution that represents the experimental energy width. In this figure, we first shifted the final theoretical cross-section curve downwards by 4 eV, in order to show a better comparison of the experimental and theoretical values for the relative heights of the resonant contributions. The 4 eV shift in energy represents less than a 0.5% of the total energy. Since our calculations did not include configuration-interaction effects, which could be significant for deep-lying subshells of heavy ions such as Sm^{12+}, a shift of 4 eV seems quite reasonable.

B. Calculations of configuration-average autoionization rates and branching ratios

A complete calculation of the height of the resonance contributions to single ionization requires detailed calculations of many energy levels, as well as level-to-level calculations of autoionization rates, radiative rates, and branching ratios. This is an extremely large and time-consuming task due to the very large number of levels that would have to be included in the calculations for a complex ion such as Sm^{12+}. Thus, we are limited here to the application of the configuration-average approximation. Even then, the calculation of branching ratios for autoionization to the many configurations of the possible final ionization stages is a formidable task. In addition, there are many problems with the configuration-average approach, arising from the fact that all the information regarding the individual levels is lost. The position of the levels within a configuration can be spread above and below an ionization limit, and the branching ratios for the individual levels can be significantly different from the configuration average branching ratios. Finally, configuration–interaction, which is not included in this approximation, can drastically change both the energy positions and the individual rates. However, by using various physical arguments in combination with our configuration-average results, we can make some useful estimates for the possible ranges of branching ratios to the various final ionization stages.

TABLE I. Main autoionization channels from the $3d^9 4s^2 4p^6 4d^{10} 4f^4 5s^2$ configuration of Sm^{11+}, to bound configurations of the Sm^{12+} ion. The energies and rates are calculated by using the CADW approximation. $X[Y]$ means $X \times 10^Y$.

Level	Configuration	Energy (eV)	Autoionization (Hz)
a	$3d^{10} 4s^2 4p^6 4d^{10} 4f^2 5s^2$ (g.s. Sm^{12+})	0.00	4.42[13]
b	$3d^{10} 4s^2 4p^6 4d^{10} 4f^3 5s$	11.35	3.46[12]
c	$3d^{10} 4s^2 4p^6 4d^{10} 4f^4$	27.53	2.52[09]
d	$3d^{10} 4s^2 4p^6 4d^9 4f^3 5s^2$	137.73	1.57[14]
e	$3d^{10} 4s^2 4p^6 4d^9 4f^4 5s$	149.13	1.39[13]

We will focus only on the first two peaks of the high-energy resonances shown in Fig. 1, that have been unambiguously identified as due to capture into the $3d^9 4s^2 4p^6 4d^{10} 4f^4 5s^2$ configuration of Sm^{11+}. Once the electron is captured, there are many paths available, as shown in Fig. 3. The dominant paths are radiative transitions to the bound levels of the Sm^{11+} ion (not shown), and autoionization to configurations of the Sm^{12+} ion. The former transitions contribute to dielectronic recombination, and the latter transitions can contribute to the resonant contributions to excitation, single ionization, or multiple ionization, according to the relative position of the final configuration of Sm^{12+}. We neglect in our calculation higher-order processes such as resonant excitation auto double ionization (READI), in which two Auger electrons are emitted simultaneously after capture [20,21]. The main radiative transitions from the $3d^9 4s^2 4p^6 4d^{10} 4f^4 5s^2$ configuration are the $3d-4f$ and the $3d-4p$ transitions, which are of the order of 10^{12} Hz and will be neglected in comparison with the higher autoionization rates. Using the excitation paths and capture strengths summarized in Fig. 3 and Tables I, II, and III, it is possible to estimate the values of the rates to the various final ionization stages, as described in the following.

The principal autoionization transitions to bound configurations of the Sm^{12+} ion are presented in Table I, and denoted a to e. The process of capture followed by autoionization to a final bound level of Sm^{12+} will ultimately contribute to resonances in the excitation cross section to that level. In order to estimate the fraction of the capture cross section that will lead to resonant contributions to excitation,

we must sum all the autoionization rates from the $3d^9 4s^2 4p^4 4d^{10} 4f^4 5s^2$ configuration to configurations lying below the Sm^{13+} ground state; this gives an autoionization rate of $\simeq 2.2 \times 10^{14}$ Hz. This must be divided by the total sum of the autoionization rates from the $3d^9 4s^2 4p^6 4d^{10} 4f^4 5s^2$ configuration, which equals $\simeq 1.25 \times 10^{15}$ Hz.

In order to calculate the portion of the capture that contributes to single ionization, we need to sum all of the autoionization rates to final configurations lying between the Sm^{13+} and Sm^{14+} ground states. The principal transitions are labeled as f to k in Table II. A more detailed treatment is required for autoionization to the configuration $3d^{10} 4s^2 4p^6 4d^8 4f^4 5s^2$ (denoted as g in the table). The autoionization rate from $3d^9 4s^2 4p^6 4d^{10} 4f^4 5s^2$ to $3d^{10} 4s^2 4p^6 4d^8 4f^4 5s^2$ is 5.6×10^{14} Hz, which is the largest rate for any of these autoionization channels. However, the autoionization rates from the $3d^{10} 4s^2 4p^6 4d^8 4f^4 5s^2$ configuration of Sm^{12} to the bound configurations of Sm^{13+} are zero, in the single-configuration approximation. Therefore, in principle, this configuration contributes to the resonant contributions to excitation and not to single ionization; however, it overlaps strongly with the configuration $3d^{10} 4s^2 4p^5 4d^{10} 4f^3 5s^2$ (f), which can autoionize strongly to the low-lying levels of Sm^{13+}. Since levels f and g have the same parity and almost the same energy, we expect very strong configuration interaction. Thus, a complete calculation of autoionization from the $3d^{10} 4s^2 4p^6 4d^8 4f^4 5s^2$ levels, including configuration-interaction, will no longer be metastable with respect to the autoionization process. In order to calculate the range of possible resonant contributions to the single-ionization cross section, we introduce a factor x that varies with the amount of mixing between the f and g configurations. We add $x \times 5.6 \times 10^{14}$ Hz to the contributions to

TABLE II. Main autoionization channels from the $3d^9 4s^2 4p^6 4d^{10} 4f^4 5s^2$ configuration of Sm^{11+}, to configurations leading to single ionization of Sm^{12+} (above the Sm^{13+} $3d^{10} 4s^2 4p^6 4d^{10} 4f 5s^2$ ground state at 226.91 eV, but below the Sm^{14+} $3d^{10} 4s^2 4p^6 4d^{10} 4f 5s$ ground state). The energies and rates are calculated by using the CADW approximation.

Level	Configuration	Energy (eV)	Autoionization (Hz)
f	$3d^{10} 4s^2 4p^5 4d^{10} 4f^3 5s^2$	271.82	1.77[13]
g	$3d^{10} 4s^2 4p^6 4d^8 4f^4 5s^2$	276.92	5.59[14]
h	$3d^{10} 4s^2 4p^5 4d^{10} 4f^4 5s$	282.24	1.14[12]
i	$3d^{10} 4s 4p^6 4d^{10} 4f^3 5s^2$	363.98	1.74[13]
j	$3d^{10} 4s 4p^6 4d^{10} 4f^4 5s$	373.49	4.22[10]
k	$3d^{10} 4s^2 4p^5 4d^9 4f^4 5s^2$	409.39	3.13[14]

TABLE III. Main autoionization channels from the $3d^9 4s^2 4p^6 4d^{10} 4f^4 5s^2$ configuration of Sm^{11+}, to configurations leading to double ionization (above the Sm^{14+} $3d^{10} 4s^2 4p^6 4d^{10} 4f 5s$ ground state, at 480.34 eV). The energies and rates are calculated by using the CADW approximation.

Level	Configuration	Energy (eV)	Autoionization (Hz)
l	$3d^{10} 4s 4p^6 4d^9 4f^4 5s^2$	501.90	8.18[13]
m	$3d^{10} 4s^2 4p^4 4d^{10} 4f^4 5s^2$	544.10	3.09[13]
n	$3d^{10} 4s 4p^5 4d^{10} 4f^4 5s^2$	633.25	8.63[12]
o	$3d^{10} 4p^6 4d^{10} 4f^4 5s^2$	730.27	2.14[10]

TABLE IV. Main autoionization channels from the $3d^{10}4s4p^64d^94f^45s^2$ configuration of Sm^{12+} (level l), calculated by using the CADW approximation. Autoionization rates for configurations of Pr^{8+}, which is isoelectronic with Sm^{12+}, are also shown. $X[Y]$ means $X \times 10^Y$.

Level	Configuration	Energy (eV)	Autoionization (Hz)
l_a	$3d^{10}4s^24p^64d^94f^25s^2$	364.78	1.69[14]
l_b	$3d^{10}4s^24p^64d^94f^35s^1$	368.60	3.52[14]
l_c	$3d^{10}4s^24p^64d^94f^4$	377.64	2.87[13]
	$3d^{10}4s^24p^64d^{10}4f5s$ (g.s. Sm^{14+})	480.24	
l_d	$3d^{10}4s^24p^64d^84f^35s^2$	504.08	3.08[14] (Pr^{8+})
l_e	$3d^{10}4s^24p^64d^84f^45s$	508.11	1.02[15] (Pr^{8+})

single ionization, and $(1-x)\times 5.6\times 10^{14}$ Hz to the resonant contributions to excitation.

To calculate the portion of the dielectronic capture that contributes to double ionization, we need to sum all the autoionization rates to final configurations lying between the Sm^{14+} and Sm^{15+} ground states. The principal transitions are labeled as l to o in Table III. More careful treatment is required for autoionization to configuration $3d^{10}4s4p^64d^94f^45s^2$ (denoted as l in the table). The autoionization rate from $3d^94s^24p^64d^{10}4f^45s^2$ to $3d^{10}4s4p^64d^94f^45s^2$ is 8.2×10^{13} Hz. The energy of this configuration is 20 eV above the Sm^{14+} ground state. The possible autoionization channels from configuration l are summarized in Table IV. The main autoionization channels from $3d^{10}4s4p^64d^94f^45s^2$ (l) that will result in double ionization are expected to be to the $3d^{10}4s^24p^64d^84f^35s^2$ configuration (l_d) and the $3d^{10}4s^24p^64d^84f^45s$ configuration (l_e). However, the configuration-average energies of these two configurations are about 2 eV and 6 eV, respectively, above configuration l. Therefore, in the CADW approximation, these further autoionization channels are closed, and configuration l, despite being above the double-ionization limit, contributes only to the single ionization cross section. Since the autoionization rates are roughly constant along an isoelectronic sequence, we can estimate the autoionization rate from configuration l to the final configurations l_d and l_e, by calculating the CADW autoionizing rates for these transitions in an ion in which they are energetically possible. For example, in Pr^{8+}, which is isoelectronic with Sm^{11+}, the autoionization rates to these levels (l_d and l_e in Table IV) are very high. We, therefore, introduce an additional factor y which represents that part of autoionization from $3d^94s^24p^64d^{10}4f^45s^2$ to $3d^{10}4s4p^64d^94f^45s^2$ that contributes to the double ionization. This factor y is a function of the fraction of levels of the $3d^{10}4s4p^64d^94f^45s^2$ configuration that are above the levels of the $3d^{10}4s^24p^64d^84f^35s^2$ and $3d^{10}4s^24p^64d^84f^45s$ configurations. If all the l levels are below the levels of l_d and l_e, then $y=0$. If all the l levels are above the levels of the l_d and l_e configurations, then according to the rates given in Table IV, the maximum value of y is 0.71.

We also analyzed other possible multiple (triple, quadruple, etc.) ionization processes that can follow the dielectronic capture to the $3d^94s^24p^64d^{10}4f^45s^2$ configuration. The $3d^{10}4s^24p^64d^{10}4f$ ground configuration of Sm^{15+} consists of two levels with an average energy of 752 eV, and in principle, the triple-ionization process (through resonant-excitation quadruple-autoionization, REQA) is energetically allowed, and has to be included in the branching-ratio calculation. We did not find in our calculations any significant autoionization rates to any configuration of Sm^{12+} lying above the 750 eV, and, therefore, for this case the REQA process, although allowed, is negligible. The $3d^{10}4s^24p^64d^{10}$ ground configuration of Sm^{16+} consists of one level at 1058 eV, 113 eV above the highest level of the $3d^94s^24p^64d^{10}4f^45s^2$ configuration (at 945 eV). Therefore, the resonant quadruple-ionization (through quintuple autoionization) is not allowed energetically.

Using this analysis, the estimated values for the processes following the dielectronic capture through the $3d^94s^24p^64d^{10}4f^45s^2$ configuration are summarized in Table V. The extreme values of the contributions to a particular final ionization stage are obtained by assuming $x=0$ and $x=1$, and $y=0$ and $y=0.7$. From these values, we can conclude that in order to obtain the REDA contribution to the single ionization, we must multiply the capture cross section by a factor between about 0.3 and about 0.8. These results are presented in Fig. 4(a), in which the experimental results

TABLE V. Summary of the estimated values of the autoionization rates for processes following the dielectronic capture through the $3d^94s^24p^64d^{10}4f^45s^2$ configuration. $X[Y]$ means $X \times 10^Y$.

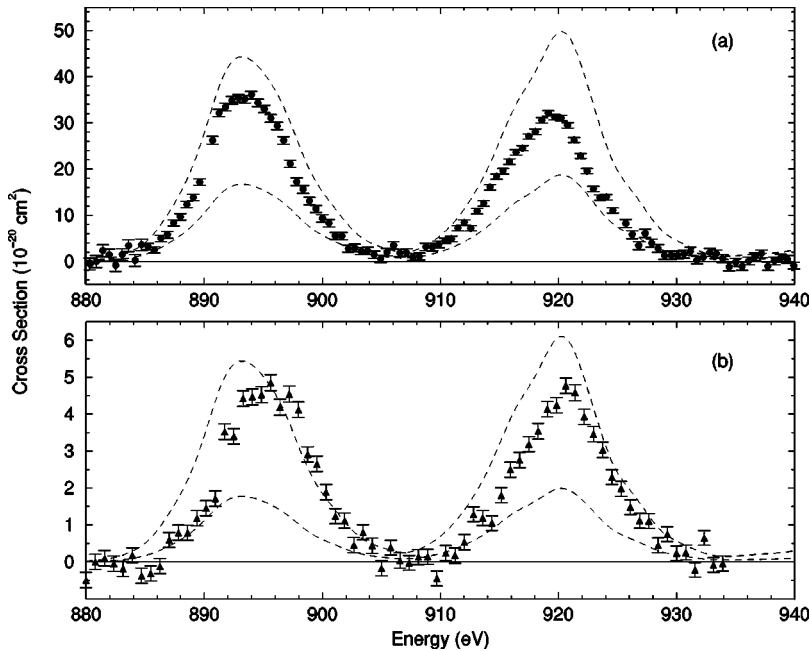| Process	Autoionization (Hz)
Total autoionization	$2.18\times 10^{14}+9.08\times 10^{14}+1.21\times 10^{14}=1.25\times 10^{15}$
Resonant excitation	$2.18\times 10^{14}+(1-x)\times 5.59\times 10^{14}$
Single ionization	$3.49\times 10^{14}+x\times 5.59\times 10^{14}+(1-y)\times 8.18\times 10^{13}$
Double ionization	$3.95\times 10^{13}+y\times 8.18\times 10^{13}$

FIG. 4. Resonant contributions to single and double electron-impact ionization of Sm^{12+}. (a): experimental measurements for single ionization. (b): experimental measurements for double ionization. The dashed curves are the extrema theoretical predictions.

are presented, together with the extreme theoretical values (dashed curves). Again, in order to facilitate the comparison, the theoretical estimations were shifted by -4 eV. We may also use the results on Table V to estimate the resonant-excitation triple-autoionization (RETA) contribution to the double ionization. Assuming that y is between 0 and 0.7, we must multiply the capture cross section by a factor 0.03 and 0.1 in order to obtain the extreme values for the double-ionization resonances. These results (with an energy shift of -4 eV) are presented in Fig. 4(b) (dashed curves).

erg are produced by deep-core inner-shell excitation with capture followed by sequential autoionization. Configuration-average distorted-wave calculations allowed us to obtain some estimates of the relative strengths of the various decay paths available after deep-core inner-shell dielectronic capture. Subsequently, we predicted a range for the size of the contribution of the dielectronic capture to the single and double-ionization cross section of Sm^{12+} and find that the experimental measurements are within these predictions.

V. CONCLUSIONS

Detailed level-to-level distorted-wave calculations of dielectronic-capture processes provide a convincing identification of the unusual high-energy resonances features found in the electron-impact ionization of the Sm^{12+} ion. The calculations include more than 13 000 levels, and show excellent agreement with the experimental results, with less than a 0.5% error in the energy position of the resonant peaks. These strong resonances features near 1000 eV incident en-

ACKNOWLEDGMENTS

[1] D.L. Moores and K.J. Reed, Adv. At., Mol., Opt. Phys. **34**, 301 (1995).

[2] K.J. LaGattuta and Y. Hahn, Phys. Rev. A **24**, 2273 (1981).

[3] K. Aichele, D. Hathiramani, F. Scheuermann, A. Müller, E. Salzborn, D. Mitnik, J. Colgan, and M.S. Pindzola, Phys. Rev. Lett. **86**, 620 (2001).

[4] M.H. Chen, K.J. Reed, and D.L. Moores, Phys. Rev. Lett. **64**, 1350 (1990).

[5] M.H. Chen and K.J. Reed, Phys. Rev. A **47**, 1874 (1993).

[6] J. Linkemann, A. Müller, J. Kenntner, D. Habs, D. Schwalm, A. Wolf, N.R. Badnell, and M.S. Pindzola, Phys. Rev. Lett. **74**, 4173 (1995).

[7] K. Tinschert, A. Müller, G. Hofmann, K. Huber, R. Becker, D.C. Gregory, and E. Salzborn, J. Phys. B **22**, 531 (1989).

[8] K. Aichele, D. Hathiramani, F. Scheuermann, A. Müller, E. Salzborn, D. M. Mitnik, D. C. Griffin, J. Colgan, and M. S. Pindzola, Phys. Rev. A **64**, 052706 (2001).

[9] R. Becker, A. Müller, C. Achenbach, K. Tinschert, and E. Salzborn, Nucl. Instrum. Methods Phys. Res. B **9**, 384 (1985).

[10] A. Müller, K. Tinschert, G. Hofmann, E. Salzborn, and G.H. Dunn, Nucl. Instrum. Methods Phys. Res. B **10/11**, 204 (1985).

[11] A. Müller, K. Tinschert, G. Hofmann, E. Salzborn, and G.H. Dunn, Phys. Rev. Lett. **61**, 70 (1988).

[12] G. Hofmann, A. Müller, K. Tinschert, and E. Salzborn, Z.

Phys. D: At., Mol. Clusters **16**, 113 (1990).

[13] K. Aichele, W. Shi, F. Scheuermann, H. Teng, E. Salzborn, and A. Müller, Phys. Rev. A **63**, 014701(R) (2000).

[14] J. Oreg, W.H. Goldstein, M. Klapisch, and A. Bar-Shalom, Phys. Rev. A **44**, 1750 (1991).

[15] M. Klapisch, J.L. Schwob, B.S. Frankel, and J. Oreg, J. Opt. Soc. Am. **67**, 148 (1977).

[16] M. Klapisch, Comput. Phys. Commun. **2**, 239 (1971).

[17] M.S. Pindzola, D.C. Griffin, and C. Bottcher, in *Atomic Pro-*

cesses in Electron-Ion and Ion-Ion Collisions, Vol. 145 of *NATO Advanced Studies Institute, Series B: Physics*, edited by F. Brouillard (Plenum, New York, 1986).

[18] R.D. Cowan, *The Theory of Atomic Structure and Spectra* (University of California, Berkeley, 1981).

[19] M.E. Riley and D.G. Truhlar, J. Chem. Phys. **63**, 2182 (1975).

[20] R.J.W. Henry and A.Z. Msezane, Phys. Rev. A **26**, 2545 (1982).

[21] M.S. Pindzola and D.C. Griffin, Phys. Rev. A **36**, 2628 (1987).